FULL PAPER

ADVANCED FUNCTIONAL MATERIALS

DOI: 10.1002/adfm.200701383

# Layered Double Hydroxide Nano- and Microstructures Grown Directly on Metal Substrates and Their Calcined Products for Application as Li-Ion Battery Electrodes**

By *Jinping Liu,** *Yuanyuan Li, Xintang Huang,** *Guangyun Li,* and *Zikun Li*

Layered double hydroxide (LDH) nano- and microstructures with controllable size and morphology have been fabricated on ''bivalent metal'' substrates such as zinc and copper by a one-step, room-temperature process, in which metal substrates act as both reactants and supports. By manipulating the concentration of $NH_3 \cdot H_2O$, the thickness and lateral size of the LDH materials can be tuned from several tens of nanometers to several hundreds of nanometers and from several hundreds of nanometers to several micrometers, respectively. This method is general and may be readily extended to any other alkali-resisted substrate coated with Zn and Cu. As an example, Zn-covered stainless steel foil has been shown to be effective for the growth of a Zn–Al LDH film. After calcinating the as-grown LDH at high temperature (650 °C) in argon gas, a $ZnO/ZnAl_2O_4$ porous nanosheet film is obtained, which is then directly used for the first time as the anode material for Li-ion batteries with the operating voltage window of 0.05–2.5 V (vs. Li). The result demonstrates that $ZnO/ZnAl_2O_4$ has higher discharge and charge capacities and considerably better cycling stability compared to pure ZnO (Li insertion/extraction rate: 200 or 500 mA $g^{-1}$). The improved electrochemical performance can be ascribed to the buffering effect of the inactive matrix $ZnAl_2O_4$ by relieving the stress caused by the volume change during charge–discharge cycling. This work represents a successful example for the development of promising ZnO-based anode materials for Li-ion batteries.

## 1. Introduction

The ability to generate advanced low-dimensional building blocks, including nanoparticles, nanorods and nanosheets, and the ability to rationally design, assemble, pattern, and integrate them into functional three-dimensional networks are crucial challenges for the development of practical nanodevices.[1,2] Over the past decade, there has been a great deal of interest in fabricating densely packed nanostructures as films on flat solid substrates.[3] Nanostructured films with controlled architectures are highly desirable for various applications in optics, electronics, biology, medicine, and energy or chemical conversions.[4] Meeting the demands of these potential applications, however, will require facile and reliable approaches for the bulk production of high-quality nanomaterials. Compared with high-temperature techniques, low-temperature solution approaches, especially those conducted at room temperature, are more attractive for their merits such as simplicity, commercial feasibility, and good potential for scale-up.[5]

Layered double hydroxides (LDHs), also known as hydrotalcite-like compounds or anionic clays, are a class of important lamellar materials.[6] They are described by the general formula $[M^{II}_{1-x}M^{III}_x(OH)_2]^{x+}[A^{m-}]_{x/m} \cdot nH_2O$ where $M^{II}$ and $M^{III}$ represent metallic cations and $A^{m-}$ the interlayer anion. The layered structure of the LDH is constructed by the periodic stacking of positively charged $(M^{II},M^{III})(OH)_2$ octahedral layers related to brucite, balanced by interlayer anions and water molecules that bind the sheets together. LDHs have gained much attention because of their wide applications as catalysts,[6] acid absorbents,[7] anion exchangers,[8] electrochemical biosensors,[9] carriers for cellular drug/gene delivery,[10] and so on. Until now, considerable attention has been directed toward the synthesis of LDH powders by well-established methods such as coprecipitation and hydrothermal synthesis.[11] The formation of LDH films is also a hot research topic in recent years. The realization of large-area uniform LDH films is especially significant to many novel applications in clay-modified electrodes, chemical or biosensors, functional coatings, and membrane catalysis.[9,12] Also, for characterization purpose, oriented LDH films

[*] Dr. J. Liu, Prof. X. Huang, Dr. Y. Li, Prof. G. Li, Dr. Z. Li
Center for Nanoscience and Nanotechnology, Department of Physics
Central China Normal University
Wuhan 430079, Hubei (P.R. China)
E-mail: liujp@phy.ccnu.edu.cn; xthuang@phy.ccnu.edu.cn
Prof. X. Huang
Key Laboratory of Ferroelectric and Piezoelectric Materials and Devices of Hubei Province
Hubei University
Wuhan 430062, Hubei (P.R. China)

[**] The authors appreciate the financial support from the National Natural Science Foundation of China (No. 50202007). The help rendered by Dr. Y. Liang and Prof. Z. J. Jia in constructing the Li-ion batteries is gratefully acknowledged. Supporting information is available online from Wiley InterScience or from the author.


WILEY InterScience DISCOVER SOMETHING GREAT
© 2008 WILEY-VCH Verlag GmbH & Co. KGaA, Weinheim

ADVANCED FUNCTIONAL MATERIALS



are very useful.[13] As a result, some effective deposition techniques have been successfully used to transfer presynthesized colloidal LDH onto various solid substrates (silicon, amorphous glass, indium tin oxide glass, various electrodes such as gold and platinum).[14,15] An important example was demonstrated in 2003 by Jung and co-workers[15] that monolayer LDH nanocrystals can be densely immobilized on silicon with their *c*-axis highly perpendicular to the substrate surface. A layer-by-layer assembly of LDH on a silicon substrate using organic acids was subsequently reported by this group.[16] Very recently, oriented self-supporting films of LDH were prepared by simple drying of LDH suspensions in glass vessels[17a] or using polystyrene (PS) colloidal crystal templates,[17b] which represents significant progress in this field.

As an alternative, Duan et al.[18] and our group[19] discovered at nearly the same time that nanostructured LDH crystals could be fabricated on an aluminum substrate in a single step. This opened up the possibility of growing large-scale uniform LDH films directly from substrates. The procedure has the advantage of being very cheap, mild, and ''green'' as it involves no organic solvents or surfactants. It is convenient that the Al foil acts as both the aluminum source and the substrate supporting the interconnected LDH. In addition, growing LDH films directly from a metal substrate considerably improves their mechanical stability and adhesion to the substrate.[18] Stimulated by these results, a general synthetic strategy for size-tunable LDH nano- or microstructures grown directly on various metal substrates has been developed in our laboratory. Like aluminum, some transition metals such as zinc and copper have high reactivity in basic solutions,[20] even at room temperature. In our experiments, the salts of zinc and copper typically used to supply bivalent metal cations are further replaced by Zn and Cu foils, while Al foil is still employed to provide trivalent $Al^{3+}$. Immersing metal foils of $M^{II}$ (Zn or Cu) and Al into a mixed aqueous solution of sodium carbonate ($Na_2CO_3$) and ammonia ($NH_3 \cdot H_2O$) at room temperature for a desired time gives LDH on Zn (or Cu) and Al. A schematic diagram of the reaction system and the involved chemical reactions are provided in the Supporting Information. Note that the growth temperature is only about 25 °C, leading to slow reaction rates; thus, the growth of LDH films is different from that observed previously.[18,19] Since the formation of LDH on an Al substrate has been well-documented, in this Full Paper, we will focus on the structures grown on ''bivalent metal'' substrates, using Zn and Cu as examples. The size and shape of the LDH can be well-tailored by the concentration of $NH_3 \cdot H_2O$ ($C_a$).

Our method can be extended with the help of mature film-coating techniques. In principle, any alkali-resisted substrate coated with these metals can be used for the growth of LDH. To demonstrate the potentials of this method, we will also show that Zn–Al LDH films can be easily prepared on Zn-coated stainless steel substrates. After being calcined at high temperature, the as-grown LDHs are completely transformed into $ZnO/ZnAl_2O_4$ compound oxides, which preserves the sheet-like shape of the LDH and the structure of which consists of numerous pores. This porous nanosheet on stainless steel is used directly as the anode material for a Li-ion battery. No additional electrode fabrication process is needed, offering several advantages such as simplicity and economy. The result indicates that spinel $ZnAl_2O_4$ species, which are electrochemically inactive with Li ions and distribute harmoniously in ZnO particle networks, appear to be successful in buffering the volume changes during dealloying–alloying processes in the electrode. As a result, the as-obtained $ZnO/ZnAl_2O_4$ products exhibit a significantly better cycling performance in comparison to pure ZnO nanomaterials.

## 2. Results and Discussion

### 2.1. Fabrication of $M^{II}$(Zn or Cu)–Al LDH Nano- and Microstructured Films

The X-ray diffraction (XRD) pattern of a Zn–Al LDH film on Zn foil prepared with $C_a = 0.06$ M is shown in Figure 1a.

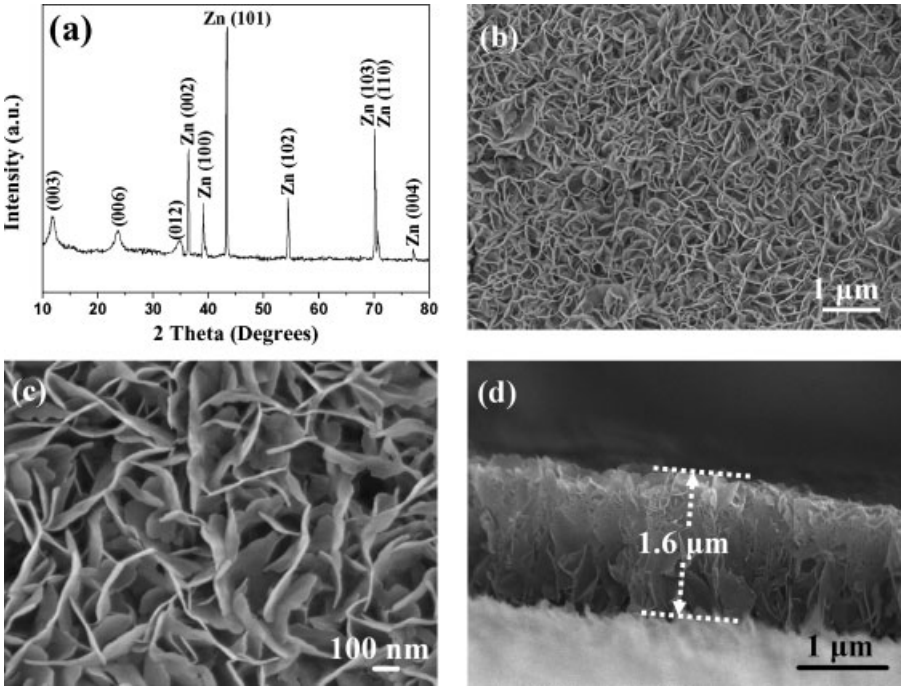


**Figure 1.** a) X-ray diffraction (XRD) pattern and b,c) scanning electron microscopy (SEM) images of a Zn–Al LDH film on Zn foil prepared with $C_a = 0.06$ M. d) Cross-sectional SEM image of the film, showing the film thickness to be approximately 1.6 μm.


© 2008 WILEY-VCH Verlag GmbH & Co. KGaA, Weinheim

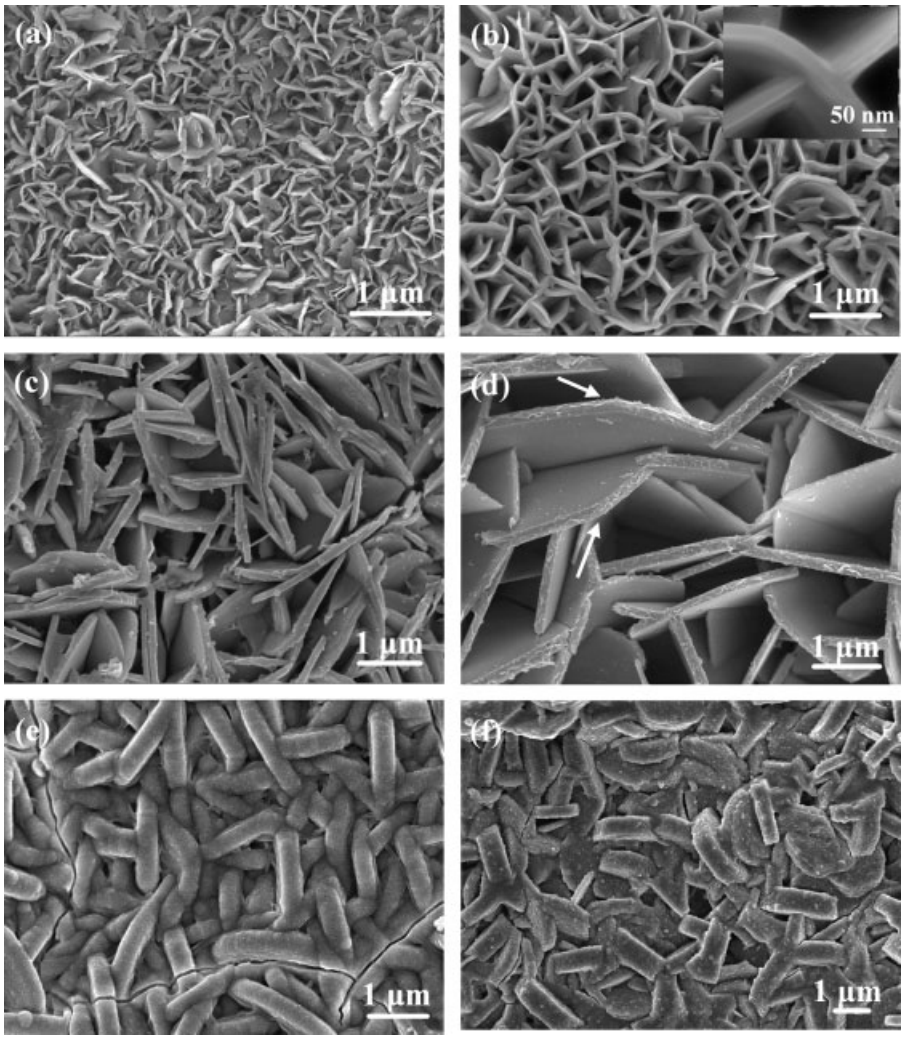


**Figure 2.** Typical SEM images of Zn–Al LDH films on Zn foil attained with different $C_a$: a) 0.10, b) 0.15, c) 0.28, d) 0.32, e) 0.41, and f) 0.50 M. The inset in (b) is an enlarged image. Arrowheads in (d) show the hexagonal shape of the LDH.

Three broad peaks centered at 11.83°, 23.67°, and 34.88 ° can be indexed to a rhombohedral Zn–Al LDH material (Joint Committee on Powder Diffraction Standards (JCPDS) file No. 48-1026), corresponding to (003), (006), and (012) planes of the LDH crystals, respectively. The appearance of (003) and (006) reflections confirms the layered structure of the LDH materials.[19] Other strong peaks are attributed to the thick polycrystalline Zn substrate (JCPDS file No. 04-0831). A Fourier transform IR (FTIR) spectrum of the product provides evidence for the presence of intercalated $(CO_3)^{2-}$ as well as water molecules (Supporting Information, Fig. S1a). Elemental analysis gives a Zn/Al molar ratio of 1.284. Based on elemental and thermogravimetric (TG) analyses, the chemical formula of LDH can be determined as $Zn_{0.56}Al_{0.44}(OH)_2(CO_3)_{0.22} \cdot 0.51H_2O$. The typical morphology of the as-prepared Zn–Al LDH film, as observed by scanning electron microscopy (SEM), is illustrated in Figure 1b and c at different magnifications. As can be seen, an LDH film with uniform density is generated on a large scale. The film consists of many interconnected flexible nanosheets with thicknesses of 10–20 nm and lateral sizes of 300–600 nm, most of which are grown with their *ab*-plane perpendicular to the substrates. A cross-sectional image of the Zn–Al-$(CO_3)^{2-}$ LDH (Fig. 1d) clearly demonstrates that the film thickness is about 1.6 μm. Another SEM image revealing the interface between the LDH film and the substrate is given in Figure S1b. From this picture, the good contact between the film and metal substrate can be observed.

The achievement of a LDH with different sizes and shapes is typically accomplished by controlling the $C_a$ parameter. The SEM images in Figure 2a–f illustrate the morphologies of Zn–Al-$(CO_3)^{2-}$ LDHs that were prepared with different $C_a$. All the size parameters of LDHs obtained under these conditions are summarized in Table 1. In general, a high $C_a$ leads to a large thickness, and the opposite applies at low or medium $C_a$. The relationship between the lateral size of LDH nano-or microstructures and $C_a$ seems complex, and a preliminary conclusion can be reached based on our experiments. That is, in the relatively high $C_a$ range (0.32–0.50 M), the lateral size decreases while increasing $C_a$; and in the low $C_a$ range (0.10–0.32 M) it increases with the increase of $C_a$. However, the lateral size may be reduced when the $C_a$ increases slightly in the very low $C_a$ range (≤0.10 M). For instance, the sheets prepared with $C_a = 0.10$ M are about 35 nm in thickness, but have lateral sizes

**Table 1.** Summarized reaction conditions and corresponding dimensions of Zn–Al LDH nano- and microstructures.

| Sample No. | $C_a$ [M] | Thickness [nm] | Lateral Size [μm] |
|---|---|---|---|
| A | 0.06 | 10–20 | 300–600 nm |
| B | 0.10 | ~35 | 220–500 nm |
| C | 0.15 | ~60 | 0.5–1 |
| D | 0.28 | 100–180 | 2–3.2 |
| E | 0.32 | 125–240 | 4–5 |
| F | 0.41 | 300–450 | 3–4.5 |
| G | 0.50 | ~600 | ~2.5 |


© 2008 WILEY-VCH Verlag GmbH & Co. KGaA, Weinheim

ADVANCED FUNCTIONAL MATERIALS



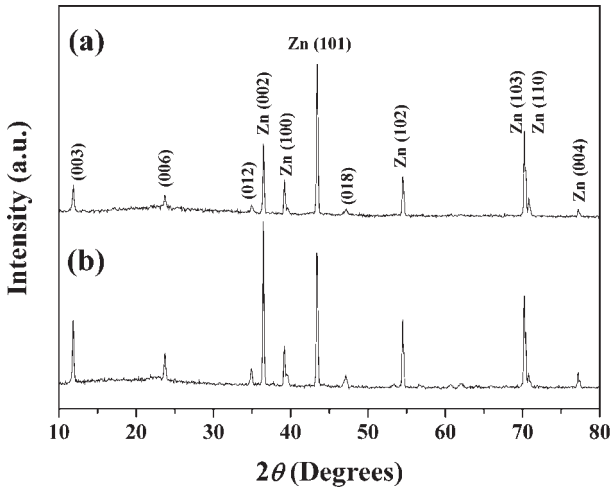


**Figure 3.** Two typical XRD results of the as-prepared Zn–Al LDH films on Zn foil by using different $C_a$: a) 0.28, b) 0.50 M.

of 220–500 nm (Fig. 2a), which are a bit smaller than those shown in Figure 1c. It can be further found that the shape of the LDH changes from curved nanosheets to nanoplatelets, and finally to disk-like crystals when $C_a$ increases. When $C_a$ reaches 0.32 M, the obtained LDHs have a hexagonal platelet-like shape with a thickness of 125–240 nm and lateral size of 4–5 μm, as shown in Figure 2d. The hexagonal morphology is thought to have developed naturally as a result of the crystallographic habit of LDH. Upon further increasing $C_a$ to 0.50 M, disk-like LDHs with very low aspect ratio are achieved (Fig. 2f). XRD results on these LDH films are selectively shown in Figure 3. Except for those peaks originating from the Zn substrate, all the observed peaks including (003), (006), (012), and (018) can be indexed to the well-known LDH materials in $(CO_3)^{2-}$ form.

For the growth of LDH, the concentration of metal cations and the pH (or basicity) were reported to be determinative.[11a,e] As suggested, relatively low concentrations of metal salts and low basicity would lead to a low degree of supersaturation, and thus a slow nucleation rate, which is favorable for the formation of LDH platelets with large size and high aspect ratio. In the present work, $NH_3 \cdot H_2O$ has two major roles. First, it reacts with metal substrates, releasing metal cations; second, it provides basic media and further adjusts the solution pH. Therefore, the above-mentioned two parameters determining the LDH growth are strongly related to $C_a$. By choosing a suitable $C_a$, these two parameters can be controlled simultaneously, directing the overall process of nucleation and crystal growth. It is believed that the growth of LDH mainly contains two simultaneous processes: the diffusional attachment of ion species to nuclei within the two-dimensional layer plane (affecting the lateral size) and the stacking growth of many layers along the *c* axis on the formed nuclei (influencing the thickness). The final shape and size of the LDH are thus determined by the synergy between these two processes. In our ''two-foil'' system, the continuous release of $Zn^{2+}$ and $Al^{3+}$ from the metal substrates by alkali etching at the beginning is a prerequisite to start the nucleation of LDH. Following this step is the formation of $Zn(OH)_4^{2-}$ and $Al(OH)_4^-$ and the diffusion of these anions under stirring. As the $Al(OH)_4^-$ ions reach the surface region of the Zn substrate, they react with $Zn(OH)_4^{2-}$ and $(CO_3)^{2-}$ at the interface, giving rise to Zn–Al-$(CO_3)^{2-}$ LDH on the Zn support. It should be pointed out that LDH nanostructures can also be found on the Al foil. However, the reaction between Al and $NH_3 \cdot H_2O$ was observed to be more drastic than that between Zn and $NH_3 \cdot H_2O$ at the early growth stage. Thus, the release and diffusion of $Al^{3+}$ were too fast, and not beneficial to the nucleation and growth of a stable LDH film on the Al substrate. Our control experiments indicated that only when the basicity was not strong and the reaction time was short, can an LDH film be obtained on the Al substrate. Figure 4a shows the SEM image of Zn–Al LDH grown on an Al foil with $C_a = 0.10$ M and a reaction time of 8 h. Nanoflakes approximately 16 nm in thickness and 100 nm in lateral size are clearly seen. The corresponding XRD pattern is displayed in Figure 4b and consists of two broad peaks of LDH and several strong peaks from the Al substrate.

Nano-or microstructured films of Cu–Al-$(CO_3)^{2-}$ LDH can also be achieved on a Cu substrate by using Cu foil instead of Zn. The growth process is very similar to that described above. $C_a$ has been used to tune the shape and size of the Cu–Al LDH structures. As shown in Figure 5a, very thin flexible nanoflakes grown on a Cu substrate can be obtained when $C_a = 0.05$ M.

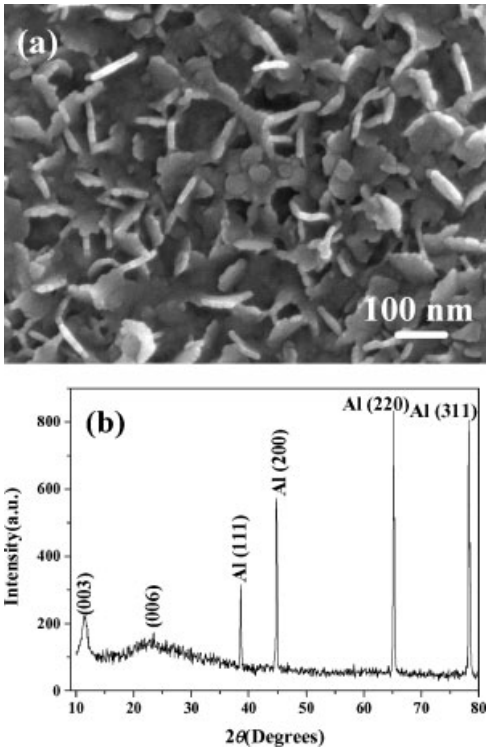


**Figure 4.** a) SEM image and b) XRD pattern of Zn–Al LDH grown on Al foil with $C_a = 0.10$ M and a reaction time of 8 h.


© 2008 WILEY-VCH Verlag GmbH & Co. KGaA, Weinheim

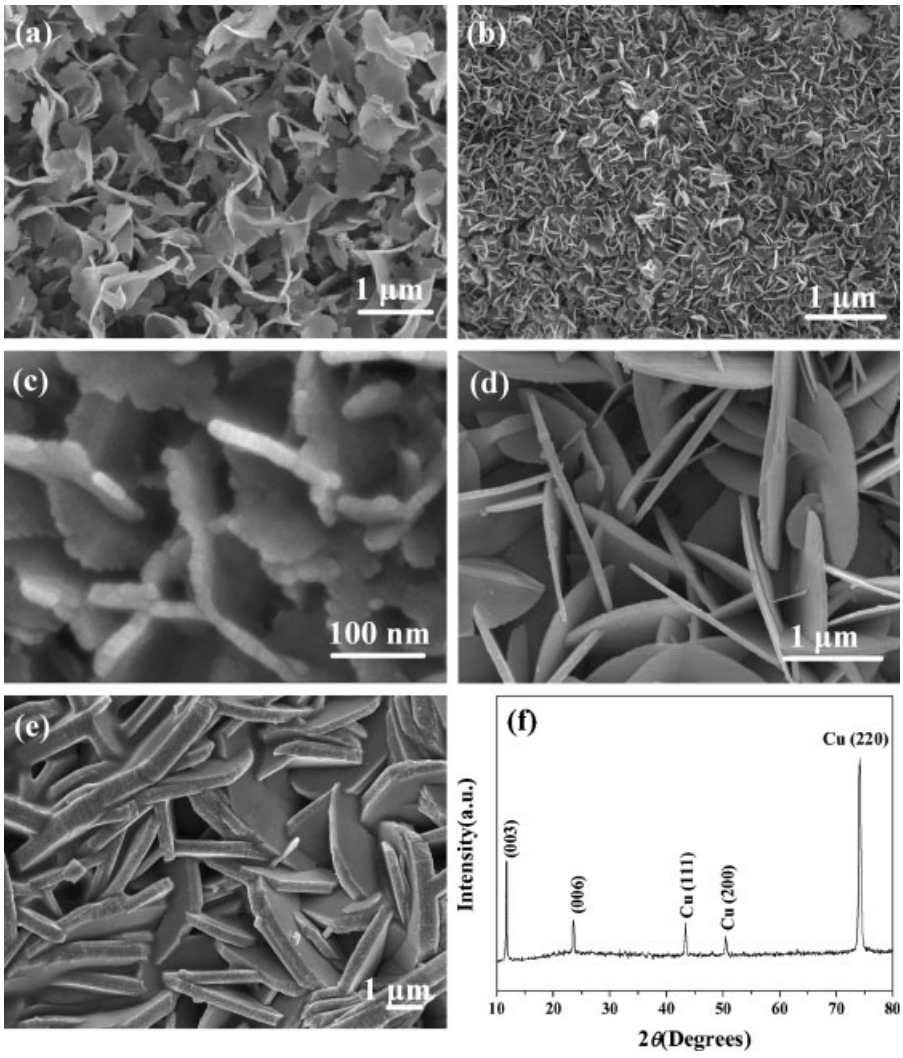


**Figure 5.** SEM images of Cu–Al LDHs grown on Cu foil by employing different $C_a$: a) 0.05, b,c) 0.085, d) 0.25, and e) 0.42 M. f) Corresponding XRD result of the Cu–Al LDH film shown in (e).

With increasing $C_a$ to 0.085 M, the shape of the Cu–Al LDH is changed: tiny nanosheets about 15–20 nm in thickness are observed in high quantity (Fig. 5b and c). A further increase in $C_a$ (0.25 M) leads to thick and large nanosheets, as shown in Figure 5d. When $C_a = 0.42$ M, hexagonal disks having a lateral size larger than 4 μm and an average thickness of 600 nm are fabricated (Fig. 5e). The corresponding XRD pattern of the hexagonal disk product is displayed in Figure 5f. Two sharp peaks in the 10°–30° range are detected, which can be indexed as pure Cu–Al LDH (JCPDS file No. 36-0630). Other observed peaks originate from the Cu substrate (JCPDS file No. 03-1005).

The structures of the as-prepared $M^{II}$(Zn or Cu)–Al-$(CO_3)^{2-}$ LDHs were further investigated by transmission electron microscopy (TEM). Zn–Al LDH flexible nanosheets prepared with $C_a = 0.06$ M are examined in Figure 6a, revealing similar sizes to those observed in SEM. Figure 6b shows the TEM image of one piece of a Zn–Al LDH platelet obtained by using 0.28 M $NH_3 \cdot H_2O$. The corresponding selected-area electron diffraction (SAED) pattern is illustrated in Figure 6c, which exhibits hexagonally arranged bright spots, confirming its good single-crystal nature. A typical TEM image of Cu–Al-$(CO_3)^{2-}$ LDH thin sheets ($C_a = 0.085$ M) and the SAED pattern are provided in Figure 6d and its inset, respectively. The single-crystal structure can also be identified. The LDH nanostructures are very sensitive to the electron-beam illumination. When we tried to obtain a high-resolution TEM image, the structure was rapidly damaged, in accordance with previous observations.[19]

In the synthesis system, no water-soluble metal salts such as zinc nitrate, copper nitrate, and aluminum nitrate were used. Thus, the effective diffusion of metal cations released from the metal foils was crucial to LDH formation. Mild stirring was employed to fulfill this need; it was expected to sufficiently mix the released bivalent and trivalent ions in the surface region of the substrates. Without stirring, only non-uniform LDH films


© 2008 WILEY-VCH Verlag GmbH & Co. KGaA, Weinheim

ADVANCED FUNCTIONAL MATERIALS



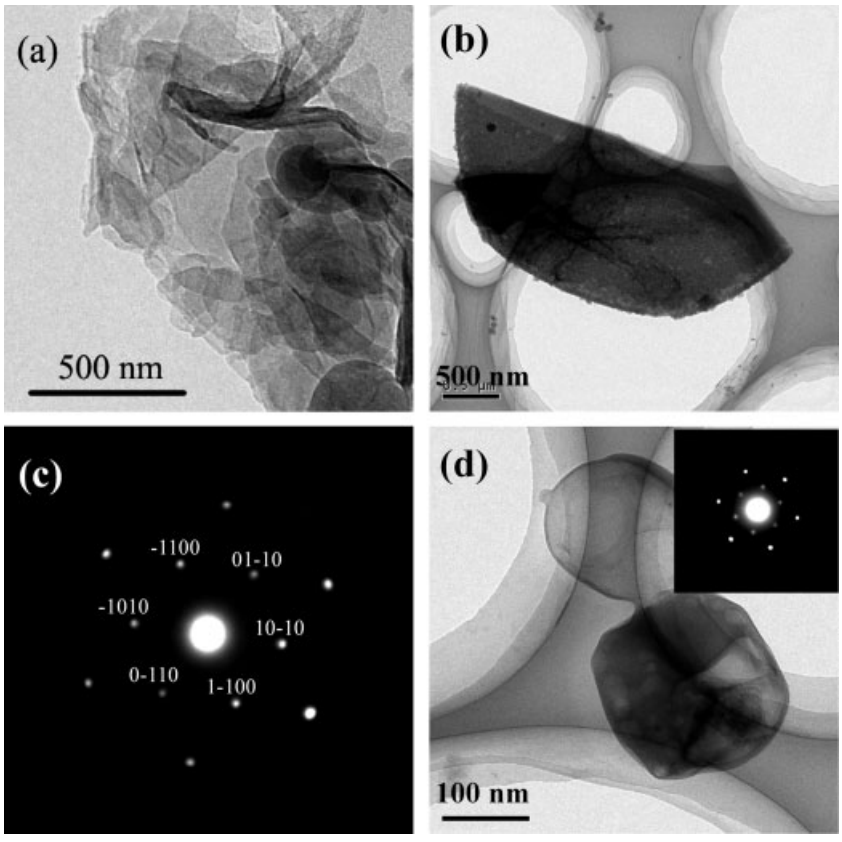


**Figure 6.** Transmission electron microscopy (TEM) images of Zn–Al LDH structures obtained with $C_a$ values of a) 0.06 and b) 0.28 M. c) Selected-area electron diffraction (SAED) pattern of the Zn–Al LDH shown in (b). d) TEM image of Cu–Al LDH nanosheets obtained by using 0.085 M ammonia. The inset shows the corresponding SAED pattern.

were obtained. Figure 7a and b illustrates two typical SEM images of Zn–Al LDH and Cu–Al LDH films fabricated in the absence of stirring, respectively, which shows that the substrates are sparsely covered.

Besides Zn and Cu foils, it seems that this procedure can be applied to any Zn or Cu film-coated substrate (metallic or nonmetallic) that is stable under basic conditions. As an example, the same synthesis of Zn–Al LDH has been demonstrated with a Zn-coated stainless steel foil, where a uniform Zn–Al LDH film directly grew on the surface (Supporting Information, Fig. S2a).

### 2.2. Formation of $ZnO/ZnAl_2O_4$ Porous Nanosheet Film from Zn–Al LDH

Calcination of LDHs is known to give oxides of divalent metal uniformly mixed with spinels.[11a,b] In LDHs, the uniform distribution of metal cations ($Zn^{2+}$ and $Al^{3+}$) on the atomic level in the brucite-like layers without segregation of ''lakes'' of separate cations facilitates the crystallization of a spinel phase upon calcination. In this work, we will use Zn–Al LDH as a model system to demonstrate the effect of calcination on the morphology variation of LDH film nano-or microstructures fabricated on metal substrates. Zn–Al-$(CO_3)^{2-}$ LDH films on stainless steel obtained with $C_a = 0.28$ and 0.50 M were subjected to calcination at 650 °C under an argon atmosphere. As revealed in Figure 8a and b (see also Supporting Information, Fig. S2b–g), the calcined products possess a very rough surface while their sheet/disk-like shape remains unchanged. Significantly, typical cross-sectional (Fig. S2f) and high-resolution top-view (Fig. S2g) SEM images clearly demonstrate that the products have good adhesion to the metal substrate, which is very important for practical applications. A typical TEM image (Fig. 8c) indicates that the calcined sheet is actually composed of many small particles, 3–10 nm in size. There are numerous pores in the structure, originating from the interparticle voids. Heating LDHs at high temperature leads to decomposition, which involves the simultaneous deanation (loss of intercalated $(CO_3)^{2-}$) and dehydroxylation of layers.[11b,19] The release of $CO_2$ and $H_2O$ gases during this process, combined with the crystallization of ZnO and spinel $ZnAl_2O_4$ nanoparticles is responsible for the formation of these voids. Energy-dispersive X-ray spectrometry (EDS) analysis in the inset of Figure 8c indicates that the particles consist of Zn, Al, and O with an atomic ratio of approximately 7:5:15. Consistent with this result, the powder XRD pattern of the resulting calcined

 © 2008 WILEY-VCH Verlag GmbH & Co. KGaA, Weinheim 

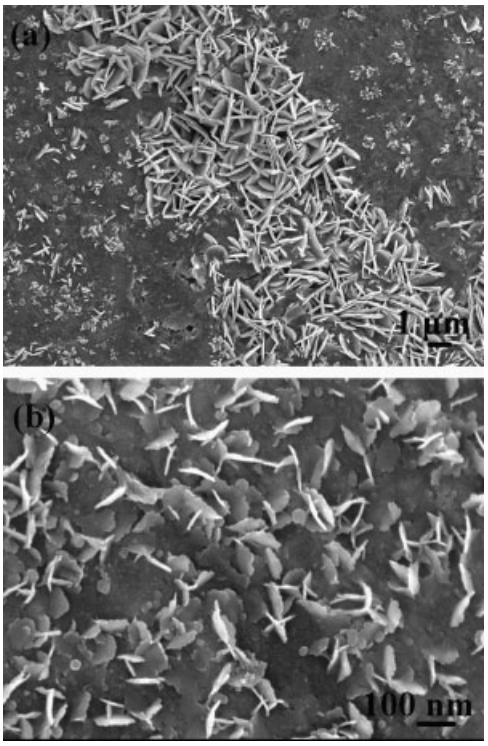


**Figure 7.** SEM images of films fabricated without stirring: a) Zn–Al LDH film on Zn foil ($C_a = 0.28$ M) and b) Cu–Al LDH film on Cu foil ($C_a = 0.085$ M).

Zn–Al LDHs (Fig. 8d) reveals that both ZnO (JCPDS file No. 36-1451) and spinel $ZnAl_2O_4$ (JCPDS file No. 05-0669) can be detected. Note that the XRD result was recorded from the powder scraped from the substrate rather than from the as-obtained compound oxide film in order to avoid the interference peaks of the substrate. Figure 8e shows a typical high-resolution TEM (HRTEM) image of the calcined product. Interplanar distances of 4.65 and 2.6 Å can be determined for two separate single-crystal particles, corresponding to the (111) plane of cubic $ZnAl_2O_4$ and the (002) facet of hexagonal ZnO, respectively. Base on the above results, it is concluded that a ZnO/$ZnAl_2O_4$ film composed of well-defined porous nanosheets is successfully obtained.

### 2.3. The Use of ZnO/$ZnAl_2O_4$ Film as Anode Material for Li-Ion Batteries

Metal oxides are the most widely investigated alternative anode materials for use in Li-ion batteries.[21] However, very little attention[22] has been directed to the use of ZnO in this field, even though it is one of the most important electronic and photonic oxide materials. The reason is that ZnO usually shows poor Li-electrochemical cyclability, resulting from volume variations during charge–discharge cycling.[22c–e] In this section, however, we will demonstrate for the first time that ZnO compounded with spinel $ZnAl_2O_4$ can show much better performance than pure ZnO when used as anode for Li-ion batteries. The obtained ZnO/$ZnAl_2O_4$ film, comprising mesoporous sheets, is suitable as a promising Li-ion battery electrode.

To evaluate the electrochemical performance of our ZnO/$ZnAl_2O_4$ compound oxides (using those attained from 0.28 M $NH_3 \cdot H_2O$ as a model system), the voltage–specific capacity curves were obtained for ''oxides on stainless steel/Li'' half-cell and its behavior is shown in Figure 9a. The cell was cycled at a rate of 200 mA $g^{-1}$ in the voltage window 0.05–2.5 V at room temperature. In Figure 9a, the voltage–capacity profiles for the 1st, 2nd, 3rd, 8th, and 10th cycle during the discharge and charge reactions are given. In order to discern the plateau voltages more clearly in the voltage profiles, the differential capacity ($dq/dV$) versus $V$ plot for the 1st cycle is further shown in the inset of Figure 9a. As can be seen, the first-specific-discharge capacity reaches a large value of approximately 1275 mA h $g^{-1}$. Another feature of interest is that the first-discharge curve can be divided into three regions, as observed in the case of other metal oxides.[21b,d,h] In the first region, the voltage drops rapidly to 1.2 V and then decreases gradually from 1.2 to 0.37 V, which corresponds to a discharge capacity of 200 mA h $g^{-1}$. It is believed that this region is closely related to the insertion of a very small amount of Li ions into the active oxides before the subsequent destruction of the crystal structure. The second and third regions, with overall capacity of 1075 mA h $g^{-1}$, comprise a large plateau at 0.35 V followed by a slope from 0.35 to 0.05 V. The observed voltage plateau is reflected as a very sharp peak in the differential capacity-versus-$V$ plot. The first-charge capacity is determined to be 590 mA h $g^{-1}$. Different from the discharge curve, the voltage profile of the 1st-charge curve only contains lines of varying slopes, confirmed by the observed four peaks in the differential capacity plot. The 1st-discharge–charge profiles qualitatively resemble those reported previously for ZnO.[22a–d] However, our total discharge and charge capacities are both larger, and our plateau voltage value of the 1st discharge is smaller. These results demonstrate that the composition and structure of ZnO-based materials play an important role in determining the electrochemical characteristics.

The 2nd-discharge profile of ZnO/$ZnAl_2O_4$ shows several slopes without an obvious voltage plateau, which is apparently different from the 1st-discharge profile. This observation indicates that the active electrode materials have changed after the 1st cycle; whereas, in the subsequent cycles, the discharge and charge profiles are very similar. As illustrated in Figure 9a, the total capacities in the 2nd discharge and charge process are about 881 and 583 mA h $g^{-1}$, respectively. Typical discharge and charge capacity values for the 10th cycle are 500 and 435 mA h $g^{-1}$, respectively. Even though there is a continuous capacity loss during the cycling process, the observed values still rank among the largest ones reported for a ZnO anode material.

As suggested, $ZnAl_2O_4$ is electrochemically inactive with Li ions.[23] The ex situ XRD pattern of the electrode collected in


© 2008 WILEY-VCH Verlag GmbH & Co. KGaA, Weinheim

ADVANCED FUNCTIONAL MATERIALS



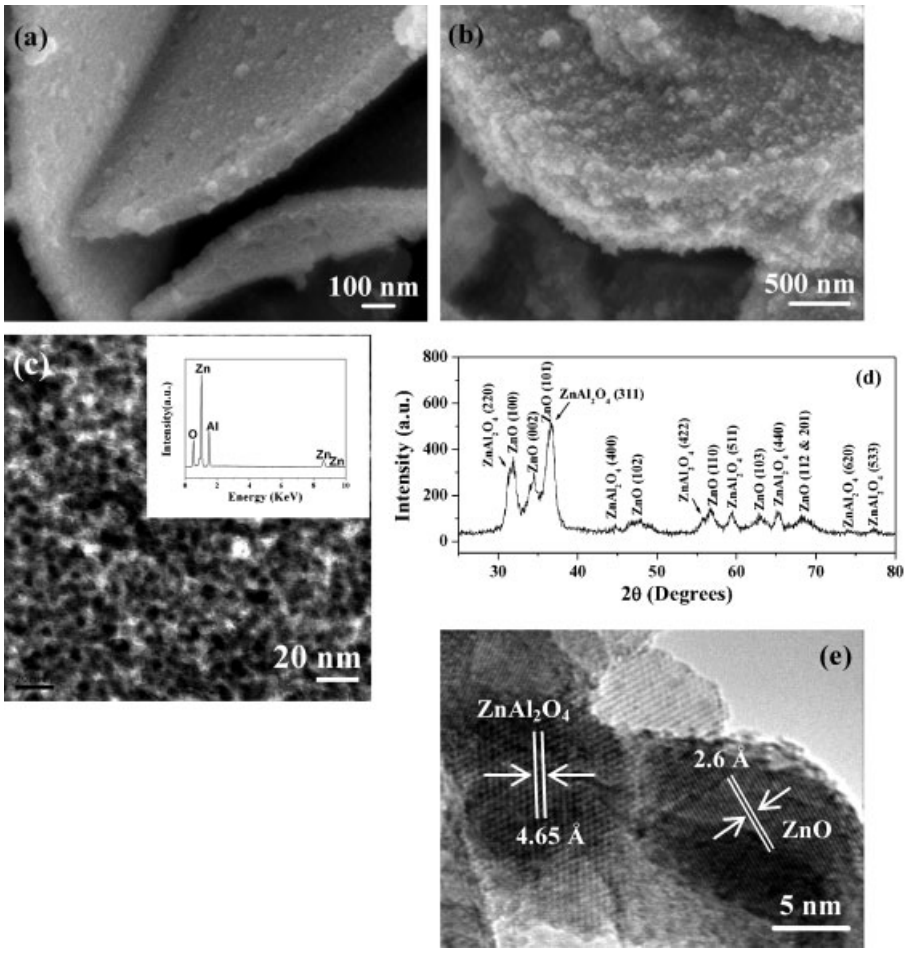


**Figure 8.** SEM images of the calcined products from Zn–Al LDH fabricated with $C_a$ values of a) 0.28 and b) 0.50 M. c) Enlarged TEM image of one sheet shown in (a). The inset is the energy dispersive X-ray spectrum. d) XRD pattern of the product shown in (a). e) High-resolution TEM (HRTEM) image of several particles observed in (c).

the fully discharged state after the 1st cycle indeed reveals the existence of crystalline $ZnAl_2O_4$; in contrast, no peaks from ZnO can be detected, which would have been caused by the electrochemical reaction with Li metal (Supporting Information, Fig. S3). From the observations outlined above and the reaction mechanism proposed in the earlier studies, the following reactions can be expected on the anode-electrode side of $ZnO/ZnAl_2O_4$–Li half cells during the 1st-discharge process:

$$ZnO + 2Li^+ + 2e^- \rightarrow Li_2O + Zn \quad (1)$$

$$Zn + Li^+ + e^- \rightarrow LiZn \quad (2)$$

When ZnO nanoparticles are electrochemically discharged with Li metal, the destruction of the crystal structure occurs followed by the formation of Zn metal ($Zn^0$) nanoparticles and $Li_2O$ (Equation 1). This process gives a large voltage plateau, as mentioned above. Upon deep discharge, Zn can further react with Li to form a Li–Zn alloy (1:1) (Equation 2). Based on the 1st-discharge reaction, the calculated theoretical capacity of ZnO would be 987.8 mA h $g^{-1}$ (i.e., three Li species per formula unit). However, the experimentally observed value is 1275 mA h $g^{-1}$, which is equivalent to approximately 3.87 Li species. The extra 0.87 Li consumption should be caused by the formation of a solid electrolyte interphase (SEI) and the polymeric gel-type layer on the Zn nanoparticles because of decomposition of the solvent in the electrolyte.[21b,i] The 1st-charge reactions are mainly represented by the reverse reaction of Equation 2 and partially reversible reaction of Equation 1, as proposed previously.[21b,22e] In particular, the three peaks in the 0–0.75 V range in the differential capacity versus $V$ plot for the 1st charge are ascribed to the average potentials for the delithiation of LiZn, which gives Zn metal ($Zn^0$) through several stages, like $LiZn \rightarrow Li_2Zn_3 \rightarrow LiZn_2 \rightarrow Li_2Zn_5$.[22a,e] A broad peak ranging from 1.0 to 1.75 V (inset in Fig. 9a) should be related to the formation of ZnO by the redox reaction between $Li_2O$ and Zn, according to the literature.[22b,21b]

In order to gain insights into the role of $ZnAl_2O_4$ inactive material in the electrode performance, pure ZnO nanosized

 © 2008 WILEY-VCH Verlag GmbH & Co. KGaA, Weinheim 

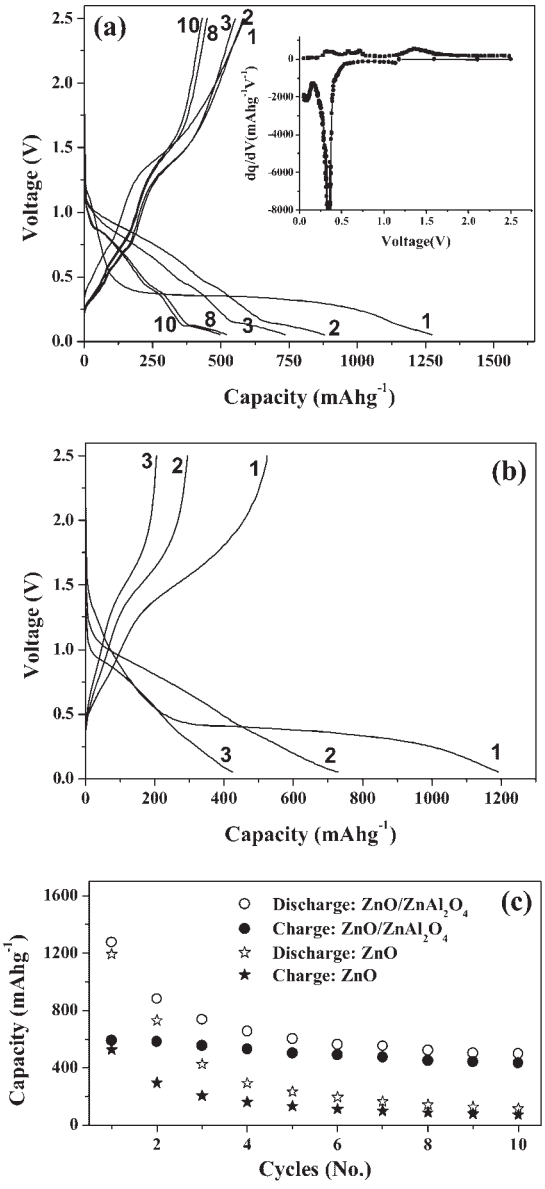


**Figure 9.** Galvanostatic charge–discharge curves of a) a $ZnO/ZnAl_2O_4$ film and b) a pure ZnO film on stainless steel in the voltage range 0.05–2.5 V (vs. Li) at a current rate of 200 mA g$^{-1}$. The numbers indicate cycle number. Inset in (a) shows the 1st-cycle differential capacity versus voltage (*V*) plots (squares: charge; circles; discharge). c) Variation in charge–discharge capacity versus cycle number for $ZnO/ZnAl_2O_4$ compound and pure ZnO.

particles on stainless steel were also prepared via a solution-phase approach followed by annealing (see Supporting Information for experimental details). ZnO nanoparticles with an average size of 8 nm were obtained, and they also constructed a porous film (Fig. S4). We evaluated the half-cell made from these particles under the same electrochemical test conditions. As can be seen in Figure 9b, even though the 1st discharge and charge capacities of the pure ZnO are still quite high, namely, 1192 and 526 mA h g$^{-1}$, respectively, its reversible capacities fade rapidly. Only 35.7% of the initial discharge capacity and 39.2% of the initial charge capacity are retained at the end of only three cycles. A fast capacity decay was also observed for other nanostructured ZnO materials, such as ball-milled particles[22d] and nanorods.[22e] For the purpose of comparison, the discharge and charge capacity versus cycle number plots up to 10 cycles for $ZnO/ZnAl_2O_4$ and ZnO are displayed in Figure 9c. It is apparent that $ZnO/ZnAl_2O_4$ exhibits a higher initial and reversible lithium storage capacity and better capacity retention than pure ZnO. The 10th discharge capacity (500 mA h g$^{-1}$) for $ZnO/ZnAl_2O_4$ is still much higher than that of graphite-based negative electrodes.

In general, the practical use of pure ZnO nanostructures as an anode for Li-ion batteries has been frustrated by the fast capacity fading of ZnO upon cycling, regardless of the size, morphology, and porosity of the nanoparticles. The severe volume changes that occur during lithium uptake and removal cannot be effectively buffered by "$Li_2O$" generated after the 1st discharge, leading to a loss of electrical contact and electrode failure. In our study, however, $ZnAl_2O_4$ may act as a robust inactive matrix. The advantages of this type of "spectator" matrix have already been discussed for tin and transition-metal-based compounds.[24] With a broad bandgap of 3.8 eV, zinc spinel $ZnAl_2O_4$ is a useful material; it can be utilized as a catalyst, dielectric, optical material, and even as a transparent conductor.[25] Benefiting from its high electrochemical stability, the existence of $ZnAl_2O_4$ in the anode results in the alleviation of the mechanical stress induced by the volume change of the active regions and can prevent the aggregation of the Zn nanograins upon cycling. All of these have beneficial effects on the electrochemical characteristics, especially on the reversible capacity retention. It should be emphasized that $ZnAl_2O_4$ particles in the present study are homogeneously dispersed in the network of ZnO nanoparticles rather than simply mixed with them, which benefits from the direct decomposition of LDH. The uniform distribution of $ZnAl_2O_4$ is a pre-requisite for effective alleviation of volume variation and thus improved cycling performance. For comparative studies, the galvanostatic cycling experiments were also conducted at the higher Li insertion/extraction rate of 500 mA g$^{-1}$. The discharge capacity versus cycle number plots still show substantial difference in the electrochemical performance between $ZnO/ZnAl_2O_4$ and ZnO, further demonstrating the essential role of $ZnAl_2O_4$ (Fig. S5). Although a more in-depth investigation of the electrochemical process is ongoing, our preliminary results show remarkable improvements in the electrochemical performance of the ZnO electrode afforded by the introduction of a novel inactive matrix. On the other hand, we should realize that the calcination temperature of LDH (factor affecting particle size and the distribution of $ZnAl_2O_4$, etc.) may influence the electrochemical properties of $ZnO/ZnAl_2O_4$ oxides. To clarify this, oxide samples prepared at different calcination temperatures (500–800 °C) were studied. In this temperature range, the obtained products always demonstrated good adhesion to the substrate. We further found that when the calcination temperature was raised from 500 to 650 °C, the


© 2008 WILEY-VCH Verlag GmbH & Co. KGaA, Weinheim

ADVANCED FUNCTIONAL MATERIALS



increase in particle size of ZnO and $ZnAl_2O_4$ was minimal. $ZnAl_2O_4$ nanoparticles were confined by highly dispersed ZnO and were prevented from recrystallizing/sintering at elevated temperatures.[11g] In this case, ZnO/$ZnAl_2O_4$ products obtained at different temperatures showed comparable electrochemical performances when used as the anode for Li-ion batteries. However, when the calcination temperature was above 650 °C, the particle size (mainly the size of $ZnAl_2O_4$) increased rapidly with the increase in temperature, consistent with previous results.[11g] TEM images of the sample attained at 800 °C are provided in the Supporting Information (Fig. S6a and b). From the HRTEM image, it can be determined that the larger and cubic particles are $ZnAl_2O_4$. The mean particle size is about 20 nm, apparently larger than that of the $ZnAl_2O_4$ synthesized by calcination at 650 °C. This demonstrates that there is partial sintering of the particles during the calcination process at 800 °C. Considering that the amount of $ZnAl_2O_4$ particles is constant, the increase in size will cause their low distribution density and distribution imhomogeneity in the compound oxides. As a result, the sample shows worse cycling performance as compared to that attained at 650 °C (Fig. S6c). Based on the above result, we can conclude that calcination temperature is crucial to the performance of $ZnAl_2O_4$ as a buffering agent.

Another good characteristic of our ZnO/$ZnAl_2O_4$-based Li-ion battery is its simplicity and low cost. Note that no conducting carbon or other additives such as binder are employed in the electrode fabrication process. The active materials are grown where the battery will later be fabricated on. There is no need to transfer the as-grown ZnO/$ZnAl_2O_4$ compound oxides to a different surface or align them; instead, the film of active materials on stainless steel can be integrated in a straightforward manner into devices as an electrode. In addition, the good adhesion of the porous sheets with each other and to the substrate (Fig.S2f and g) can facilitate the maintenance of the electrode integrity in spite of the occurrence of Li uptake and removal.

## 3. Conclusions

In summary, we have successfully developed a room-temperature immersion method to fabricate LDH with tunable structures on different metal foils. This one-step synthesis, employing two foils instead of metal salts, has proven to be straightforward and remarkably versatile, especially for the facile growth of LDH on ''bivalent metal'' substrates such as Zn and Cu. In particular, benefiting from the mature film coating techniques, alkali-resisted substrates coated with Zn and Cu are expected to be competent for the growth of LDH. A good example has been demonstrated by using a Zn-coated stainless steel foil to grow a Zn–Al LDH film. The direct realization of LDH on metal substrates has various advantages for practical applications. Herein we demonstrate the first usage of a calcined LDH film on stainless steel foil as an anode for Li-ion batteries. The most important aspect is the ability to directly integrate the as-obtained ZnO/$ZnAl_2O_4$ porous film into the battery device, offering significant advantages with respect to cost and practicability. As demonstrated, our ZnO/$ZnAl_2O_4$ exhibits a first discharge capacity of 1275 mA h $g^{-1}$ and a discharge capacity of 500 mA h $g^{-1}$ after 10 cycles, with pronounced improvement of cycling stability, as compared to pure ZnO. The improved electrochemical performance can be ascribed to the $ZnAl_2O_4$ inactive matrix. Our work offers exciting possibilities for the development of new anode materials for Li-ion batteries.

## 4. Experimental

All of the reagents were purchased from Shanghai Chemical Reagent Co., Ltd. The Zn-coated stainless steel substrate was prepared by a vacuum-deposition technique using Zn as the evaporating target material (machine type: DM-450A, the thickness of stainless steel was ca. 0.15 mm, Zn film thickness was ca. 3 μm). All of the substrates were cleaned with ethanol and distilled water before use. For the growth of LDH nano- and microstructures, typically, a Zn foil (purity: ca. 99%, 30 mm × 30 mm × 0.25 mm, or Cu, Zn-coated stainless steel) and an Al foil (purity: ca. 99%, 30 mm × 30 mm × 0.15 mm) were suspended simultaneously into a mixed aqueous solution (200 mL) containing $Na_2CO_3$ ($1.68 \times 10^{-2}$ M) and $NH_3 \cdot H_2O$ (tunable concentration) at room temperature (25 °C) for three days. After the reaction, the foils were taken out of the solution, washed with distilled water and dried at 60 °C.

The products were characterized using powder X-ray diffraction (Bruker D-8 Avance, Cu K$\alpha$ radiation; $\lambda = 1.5418$ Å), transmission electron microscopy (TEM and HRTEM, JEM-2010FEF, 200 kV), and scanning electron microscopy (SEM, JSM-6700F, 5.0 kV) equipped with an energy-dispersive X-ray spectrometer. Fourier transform IR (FTIR) spectra were recorded on a NICOLET NEXUS470 Fourier transform infrared spectrometer. TG analysis was carried out on an SDT600 apparatus with a heating rate of 10 °C $min^{-1}$ in $N_2$ atmosphere. For the electrochemical performance test, the ZnO/$ZnAl_2O_4$ film was derived from LDH on stainless steel fabricated with $C_a = 0.28$ M. The cell was assembled in an argon-filled glove box (Mbraun, Unilab, Germany)[21b] by directly using the as-obtained film as the anode, a Li-metal circular foil (0.59 mm thick, 14 mm diameter) as the counter and reference electrodes, a microporous polypropylene membrane as the separator, and 1 M solution of $LiPF_6$ in ethylene carbonate (EC) and diethyl carbonate (DEC) (1:1 by volume) as the electrolyte. The cell was aged for 7 h before measurement. The charge–discharge cycling was performed at room temperature by using a multichannel battery tester (model SCN, Bitrode, USA). The capacity values were determined based on the quantity of active ZnO. For doing ex situ XRD, the cell obtained after the 1st discharge was dismantled in the glove box. The anode was then washed thoroughly to remove the remaining electrolyte and dried at 65 °C in vacuum.

Received: November 28, 2007
Revised: January 20, 2008

[1] *The Chemistry of Nanomaterials: Synthesis, Properties and Applications* (Eds: C. N. R. Rao, A. Müller, A. K. Cheetham), Wiley-VCH, Weinheim, Germany **2004**.

[2] L. Vayssieres, A. Manthiram, in *Encyclopedia of Nanoscience and Nanotechnology*, Vol. 8 (Eds: H. S. Nalwa), American Scientific, Stevenson Ranch, CA **2004**, pp. 147–166.

 © 2008 WILEY-VCH Verlag GmbH & Co. KGaA, Weinheim 

[3] J. H. Fendler, *Nanoparticles and Nanostructured Films: Preparation, Characterization and Applications*, John Wiley, New York **1998**.
[4] T. L. Sounart, J. Liu, J. A. Voigt, J. W. P. Hsu, E. D. Spoerke, Z. R. Tian, Y. B. Jiang, *Adv. Funct. Mater.* **2006**, *16*, 335.
[5] a) L. E. Greene, M. Law, J. Goldberger, F. Kim, J. C. Johnson, Y. F. Zhang, R. J. Saykally, P. Yang, *Angew. Chem. Int. Ed.* **2003**, *42*, 3031. b) L. Vayssieres, K. Keis, S. E. Lindquist, A. Hagfeldt, *J. Phys. Chem. B* **2001**, *105*, 3350. c) L. Vayssieres, *Adv. Mater.* **2003**, *15*, 464. d) G. Z. Shen, D. Chen, *J. Am. Chem. Soc.* **2006**, *128*, 11 762.
[6] a) B. Sels, D. De Vos, M. Buntinx, F. Pierard, A. Kirsch-De Mesmaeker, P. Jacobs, *Nature* **1999**, *400*, 855. b) W. Kagunya, Z. Hassan, W. Jones, *Inorg. Chem.* **1996**, *35*, 5970. c) V. R. Choudhary, D. K. Dumbre, B. S. Uphade, V. S. Narkhede, *J. Mol. Catal. A: Chem.* **2004**, *215*, 129. d) L. Ren, J. He, S. Zhang, D. G. Evans, X. Duan, *J. Mol. Catal. B: Enzym.* **2002**, *18*, 3.
[7] a) P. C. Pavan, G. Gomes, J. B. Valim, *Microporous Mesoporous Mater.* **1998**, *21*, 659. b) L. Lv, J. He, M. Wei, D. G. Evans, X. Duan, *Water Res.* **2006**, *40*, 735.
[8] a) D. L. Bish, *Bull. Mineral.* **1980**, *103*, 170. b) G. R. Williams, D. O'Hare, *Chem. Mater.* **2005**, *17*, 2632. c) R. P. Bontchev, S. Liu, J. L. Kumhansl, J. Vogit, T. M. Nenoff, *Chem. Mater.* **2003**, *15*, 3669. d) A. I. Khan, D. O'Hare, *J. Mater. Chem.* **2002**, *12*, 3191.
[9] a) D. Shan, W. J. Yao, H. G. Xue, *Electroanalysis* **2006**, *18*, 1485. b) D. Shan, C. Mousty, S. Cosnier, *Anal. Chem.* **2004**, *76*, 178.
[10] a) M. Darder, M. López-Blanco, P. Aranda, F. Leroux, E. Ruiz-Hitzky, *Chem. Mater.* **2005**, *17*, 1969. b) L. Desigaux, M. B. Belkacem, P. Richard, J. Cellier, P. Léone, L. Cario, F. Leroux, C. Taviot-Guého, B. Pitard, *Nano Lett.* **2006**, *6*, 199. c) Q. Yuan, M. Wei, D. G. Evans, X. Duan, *J. Phys. Chem. B* **2004**, *108* 12 381.
[11] a) D. G. Evans, X. Duan, *Chem. Commun.* **2006**, 485. b) F. Cavani, F. Trifirò, A. Vaccari, *Catal. Today* **1991**, *11*, 173. c) L. Hickey, J. T. Kloprogge, R. L. Frost, *J. Mater. Sci.* **2000**, *35*, 4347. d) S. Abelló, J. Pérez-Ramírez, *Adv. Mater.* **2006**, *18*, 2436. e) Z. Liu, R. Ma, M. Osada, N. Iyi, Y. Ebina, K. Takada, T. Sasaki, *J. Am. Chem. Soc.* **2006**, *128*, 4872. f) R. Ma, Z. Liu, K. Takada, N. Iyi, Y. Bando, T. Sasaki, *J. Am. Chem. Soc.* **2007**, *129*, 5257. g) L. Zou, F. Li, X. Xiang, D. G. Evans, X. Duan, *Chem. Mater.* **2006**, *18*, 5852.
[12] a) R. B. Leggat, S. A. Taylor, S. R. Taylor, *Colloids Surf. A* **2002**, *210*, 83. b) J. X. He, K. Kobayashi, M. Takahashi, G. Villemure, A. Yamagishi, *Thin Solid Films* **2001**, *397*, 225. c) R. G. Buchheit, H. Cuan, *JCT Res.* **2004**, *1*, 277.
[13] P. S. Bratterman, C. Q. Tan, J. X. Zhao, *Mater. Res. Bull.* **1994**, *29*, 1217.
[14] a) E. Gardner, K. M. Huntoon, T. J. Pinnavaia, *Adv. Mater.* **2001**, *13*, 1263. b) J. Qiu, G. Villemure, *J. Electroanal. Chem.* **1995**, *359*, 159. c) R. Roto, A. Yamagishi, G. Villemure, *J. Electroanal. Chem.* **2004**, *572*, 101. d) Y. F. Gao, M. Nagai, Y. Masuda, F. Sato, W. S. Seo, K. Koumoto, *Langmuir* **2006**, *22*, 3521. e) X. D. Lei, L. Yang, F. Z. Zhang, D. G. Evans, X. Duan, *Chem. Lett.* **2005**, *34*, 1610.
[15] a) J. H. Lee, S. W. Rhee, D. Y. Jung, *Chem. Commun.* **2003**, 2740. b) J. H. Lee, S. W. Rhee, D. Y. Jung, *Chem. Mater.* **2004**, *16*, 3774.
[16] J. H. Lee, S. W. Rhee, D.-Y. Jung, *J. Am. Chem. Soc.* **2007**, *129*, 3522.
[17] a) L. Y. Wang, C. Li, M. Liu, D. G. Evans, X. Duan, *Chem. Commun.* **2007**, 123. b) E. Géraud, V. Pévot, J. Ghanbaja, F. Leroux, *Chem. Mater.* **2006**, *18*, 238.
[18] H. Y. Chen, F. Z. Zhang, S. S. Fu, X. Duan, *Adv. Mater.* **2006**, *18*, 3089.
[19] J. P. Liu, X. T. Huang, Y. Y. Li, K. M. Sulieman, X. He, F. L. Sun, *J. Phys. Chem. B* **2006**, *110*, 21 865.
[20] a) Y. P. Fang, Q. Pang, X. G. Wen, J. N. Wang, S. H. Yang, *Small* **2006**, *2*, 612. b) J. P. Liu, X. T. Huang, Y. Y. Li, K. M. Sulieman, X. He, F. L. Sun, *J. Mater. Chem.* **2006**, *16*, 4427.
[21] a) *Lithium Batteries — Science and Technology* (Eds: G. A. Nazri, G. Pistoia), Kluwer Academic, New York **2003**. b) Y. Sharma, N. Sharma, C. V. S. Rao, B. V. R. Chowdari, *Adv. Funct. Mater.* **2007**, *17*, 2855. c) Z. H. Wen, Q. Wang, Q. Zhang, J. H. Li, *Adv. Funct. Mater.* **2007**, *17*, 2772. d) W.-Y. Li, L.-N. Xu, J. Chen, *Adv. Funct. Mater.* **2005**, *15*, 851. e) D. H. Park, S.-H. Lee, T. W. Kim, S. T. Lim, S.-J. Hwang, Y. S. Yoon, Y.-H. Lee, J.-H. Choy, *Adv. Funct. Mater.* **2007**, *17*, 2949. f) Y. Wang, K. Takahashi, K. Lee, G. Z. Cao, *Adv. Funct. Mater.* **2006**, *16*, 1133. g) Y. Wang, H. C. Zeng, J. Y. Lee, *Adv. Mater.* **2006**, *18*, 645. h) S. Han, B. Jang, T. Kim, S. M. Oh, T. Hyeon, *Adv. Funct. Mater.* **2005**, *15*, 1845. i) M. V. Reddy, T. Yu, C. H. Sow, Z. X. Shen, C. T. Lim, G. V. Subba Rao, B. V. R. Chowdari, *Adv. Funct. Mater.* **2007**, *17*, 2792.
[22] a) J. Wang, P. King, R. A. Huggins, *Solid State Ionics* **1986**, *20*, 185. b) H. Li, X. Huang, L. Chen, *Solid State Ionics* **1999**, *123*, 189. c) F. Belliard, P. A. Connor, J. T. S. Irvine, *Solid State Ionics* **2000**, *135*, 163. d) F. Belliard, J. T. S. Irvine, *J. Power Sources* **2001**, *97–98*, 219. e) Z. F. Zheng, X. P. Gao, G. L. Pan, J. L. Bao, J. Q. Qu, F. Wu, D. Y. Song, *Chin. J. Inorg. Chem.* **2004**, *20*, 488.
[23] M. Hibino, M. Nakamura, Y. Kamitaka, N. Ozawa, T. Yao, *Solid State Ionics* **2006**, *177*, 2653.
[24] a) N. Sharma, K. M. Shaju, G. V. S. Rao, B. V. R. Chowdari, *Electrochem. Commun.* **2002**, *4*, 947. b) N. Sharma, K. M. Shaju, G. V. S. Rao, B. V. R. Chowdari, Z. L. Dong, T. J. White, *Chem. Mater.* **2004**, *16*, 504. c) N. Sharma, K. M. Shaju, G. V. S. Rao, B. V. R. Chowdari, *Electrochim. Acta* **2004**, *49*, 1035.
[25] a) H. J. Fan, M. Knez, R. Scholz, K. Nielsch, E. Pippel, D. Hesse, M. Zacharis, U. Gosele, *Nat. Mater.* **2006**, *5*, 627. b) Y. Wang, Q. Liao, H. Lei, X. P. Zhang, X. C. Ai, J. P. Zhang, K. Wu, *Adv. Mater.* **2006**, *18*, 943, and references therein.


© 2008 WILEY-VCH Verlag GmbH & Co. KGaA, Weinheim